

Reconstructing an Icosahedral Virus from Single-Particle Diffraction Experiments

D. K. Saldin, H.-C. Poon, P. Schwander, M. Uddin, and M. Schmidt

*Department of Physics, University of Wisconsin-Milwaukee, P. O. Box 413,
Milwaukee, WI 53201*

dksaldin@uwm.edu

Abstract:

The first experimental data from single-particle scattering experiments from free electron lasers (FELs) are now becoming available. The first such experiments are being performed on relatively large objects such as viruses, which produce relatively low-resolution, low-noise diffraction patterns in so-called “diffract-and-destroy” experiments. We describe a very simple test on the angular correlations of measured diffraction data to determine if the scattering is from an icosahedral particle. If this is confirmed, the efficient algorithm proposed can then combine diffraction data from multiple shots of particles in random unknown orientations to generate a full 3D image of the icosahedral particle. We demonstrate this with a simulation for the satellite tobacco necrosis virus (STNV), the atomic coordinates of whose asymmetric unit is given in Protein Data Bank entry 2BUK.

© 2018 Optical Society of America

OCIS codes: (100.3200) Image Processing: Inverse Scattering; (190.5825) Scattering: Scattering Theory.

References and links

1. R. Neutze, R. Wouts, D. van der Spoel, E. Weckert, and J. Hajdu, “Potential for biomolecular imaging with femtosecond X-ray pulses”, *Nature* **406**, 752-757 (2000).
2. M. M. Seubert et al., “Single mimivirus particles intercepted and imaged with an X-ray laser,” *Nature* **470**, 78–81 (2011).
3. V. L. Shneerson, A. Ourmazd, and D. K. Saldin, “Crystallography without crystals I: the common-line method for assembling a 3D diffraction volume from single-particle scattering”, *Acta Cryst. A* **64**, 303-315 (2008).
4. R. Fung, V. L. Shneerson, D. K. Saldin, and A. Ourmazd, “Structure from fleeting illumination of faint spinning objects in flight”, *Nature Physics* **5**, 64-67 (2009).
5. N.-T. D. Loh and V. Elser, “Reconstruction algorithm for single-particle diffraction imaging experiments”, *Phys. Rev. E* **80**, 026705 (2009).
6. D. K. Saldin, V. L. Shneerson, R. Fung, and A. Ourmazd, “Structure of isolated biomolecules from ultrashort x-ray pulses: exploiting the symmetry of random orientations”, *J. Phys: Condens. Matter* (2009).
7. Z. Kam, “Determination of macromolecular structure in solution by spatial correlation of scattering fluctuations”, *Macromolecules* **10**, 927-934 (1977).
8. R. A. Kirian, K. E. Schmidt, and J. C. H. Spence, “Signal, noise, and resolution in correlated fluctuations from snapshot SAXS”, submitted for publication (2011).
9. D. L. D. Caspar and A. Klug, “Physical principles in the construction of regular viruses”, *Cold Spring Harbor Symp. Quant. Biol.* **27**, 1-24 (1962).
10. A. Jack and S. C. Harrison, “On the interpretation of small-angle x-ray solution scattering from spherical viruses”, *J. Mol. Biol.* **99**, 15-25 (1975).

11. Z. Kam, "The reconstruction of structure from electron micrographs of randomly oriented particles", *J. theor. Biol.* **82**, 15-39 (1980).
12. D. K. Saldin, H. C. Poon, V. L. Shneerson, M. Howells, H. N. Chapman, R. Kirian, K. E. Schmidt, and J. C. H. Spence, "Beyond small angle x-ray scattering: exploiting angular correlations", *Phys. Rev. B* **81**, 174105 (2010).
13. J. Miao, P. Charalambous, J. Kirz, and D. Sayre, "Extending the methodology of X-ray crystallography to allow imaging of micrometer-sized non-crystalline specimens", *Nature* **400**, 342-344 (1999).
14. S. Marchesini, "A unified evaluation of iterative projection algorithms for phase retrieval", *Rev. Sci. Instrum.* **78**, 049901 (2007).
15. See e.g. the Wikipedia entry at <http://en.wikipedia.org/wiki/Icosahedron>
16. D. A. Varshalovich, A. N. Moskalev, and V. K. Khersonskii, *Quantum Theory of Angular Momentum*, (World Scientific, 1988), p.148.
17. P. J. Davis and P. Rabinowitz, *Methods of Numerical Integration*, 2nd Ed. (Dover Publications, 1984).
18. L. Lovisolo and E. A. B. Da Silva, "Uniform distribution of points on a hyper-sphere with applications to vector bit-plane encoding", *IEEE Proc. Vis. Image Signal Process.* **148**, 187-193 (2001).
19. H. C. Poon and D. K. Saldin, "Beyond the crystallization paradigm: structure determination from diffraction patterns of ensembles of randomly oriented particles", *Ultramicrosc.* **111**, 798-806 (2011).
20. C. Xiao, P. R. Chipman, A. J. Battisti, V. D. Bowman, P. Renesto, D. Raoult, and M. G. Rossmann, "Cryo-electron microscopy of the giant mimivirus", *J. Mol. Biol.* **353**, i493-496 (2005).
21. M. V. Cherrier, C. A. Xiao, V. D. Bowman, A. J. Battisti, X. D. Yan, P. R. Chipman, T. S. Baker, J. L. van Etten, and M. G. Rossmann, "An icosahedral algal virus has a complex unique vertex decorated by a spike", *PNAS* **106**, 11085-11089 (2009).
22. G. Oszlanyi and A. Suto, "Ab initio structure solution by charge flipping", *Acta Cryst.* **A60**, 134-141 (2004).
23. G. Oszlanyi and A. Suto, "Ab initio structure solution by charge flipping. II. Use of weak reflections", *Acta Cryst.* **A61**, 147-152 (2005).
24. Y. Zheng, P. C. Doerschuk, and J. E. Johnson, "Determination of three-dimensional low-resolution viral structure from solution X-ray scattering data", *Biophys. J.* **69**, 619-639 (1995).
25. VIPERdb, a database for icosahedral virus capsid structures may be accessed at <http://viperdb.scripps.edu>. As of May 5, 2011, it contained 298 icosahedral viruses, of which the structures of 265 has been determined by x-ray diffraction, and 33 by cryo electron microscopy.
26. J. B. Pendry, *Low Energy Electron Diffraction*, (Academic Press, 1974).
27. D. K. Saldin, V. L. Shneerson, M. Howells, S. Marchesini, H. N. Chapman, R. Kirian, K. E. Schmidt, and J. C. H. Spence, "Structure of a single particle from scattering of many particles randomly oriented about an axis: towards structure solution without crystallization?", *New J. Phys.* **12**, 035014 (2010).
28. D. K. Saldin, H. C. Poon, M. Bogan, S. Marchesini, D. A. Shapiro, R. A. Kirian, U. Weierstall, and J. C. H. Spence, "New light on disordered ensembles: ab-initio structure determination of one particle from scattering fluctuations of many copies", *Phys. Rev. Lett.* **106**, 115501 (2011).
29. D. De Ponte, R. B. Doak, P. Fromme, G. Hembree, M. Hunter, S. Marchesini, K. E. Schmidt, U. Weierstall, and J. C. H. Spence, *J. Synch. Rad.* **15**, 593-599 (2008).

1. Introduction

The free electron lasers (FELs) now beginning to come online produce radiation many orders of magnitude brighter than any existing source, and enable experiments previously the domain only of science fiction. One such proposed experiment [1] envisages reconstructing the 3D structure of a microscopic entity such as a virus from many ultrashort diffraction patterns of many identical copies of the particles in random orientations from single pulses of FEL radiation. Although the particles will undoubtedly suffer catastrophic radiation damage, the ultrashort nature of FEL radiation is expected to produce diffraction patterns of the particles before significant disintegration. An experiment on individual mimivirus particles was reported recently [2]. The paper illustrates convincing diffraction patterns of the virus particle in two different orientations, from which 2D projections of the particles are reconstructed using an iterative phasing algorithm. Although such particles are known to be largely icosahedral, little evidence of the icosahedral shape is evident in the reconstructed projections. Several algorithms have been proposed for reconstructing a full 3D image of the particle from an ensemble of many such diffraction patterns from randomly oriented particles. The methodology followed by some of these approaches [3, 4, 5] is to find the likely orientation of the measured diffraction patterns in the 3D reciprocal space of the particle.

Another approach [6] dispenses with finding the likely orientations of the individual diffraction patterns by integrating over orientations, in an attempt to find the spherical harmonic representation of the 3D diffraction volume of a single particle from the averages of the angular correlations of the intensities on the measured diffraction patterns. This method of analysis is even applicable to individual diffraction patterns from multiple identical particles [7]. The particles need to be frozen in space or time while the scattering is taking place. If the scattering is from a single FEL pulse of radiation, the particles will be essentially frozen in time for the duration of the scattering even if not frozen in space. This opens this method to the analysis of scattering from particles in random orientations within a droplet. With such an approach, the “hit rate” in an experiment with a FEL can become 100%, whereas a low hit rate is to be expected when attempting to hit submicron particles with a submicron pulsed laser beam. The signal-to-noise ratio from such snapshot patterns is independent of the number of particles per shot, but increases with the square root of the number of shots [8]. This approach also has the advantage that it operates on a compressed version of the voluminous data produced by a FEL.

We point out here another advantage of this approach: it is easily amenable to simplifications resulting from any known point-group symmetry of the particles under study. This is a powerful advantage for the study of virus structure, which is dominated by that of its protein coat which encloses the genetic material, DNA or RNA, which contain the instructions for the replication of the virus. To quote from Caspar and Klug [9] “there are only a limited number of efficient designs possible for a biological container which can be constructed from a large number of identical protein molecules, The two basic designs are helical tubes and icosahedral shells”. Viruses have regular shapes since they are formed by the self assembly of identical protein subunits which are coded by the limited quantity of genetic material capable of being stored within the small volume enclosed by its protein coat. An icosahedron, for example can be formed by the self assembly of at least 60 identical subunits. The genetic material needs to code for just one of these subunits, a factor of at least 60 smaller than the entire structure.

2. Icosahedral Harmonics

The first aim of this approach is to find the spherical harmonic representation of the intensity distribution of any resolution shell in the reciprocal space of a single particle. Any prior information about the nature of this distribution may be incorporated by limiting the set of spherical harmonics over which the summation is performed and by any relationship amongst the amplitudes of the different spherical harmonics which are a consequence of any known point-group symmetry.

An obvious restriction of the form of the intensity distribution

$$I(q, \theta, \phi) = \sum_{lm} I_{lm}(q) Y_l^m(\theta, \phi) \quad (1)$$

is its known inversion (or Friedel) symmetry. Since

$$Y_l^m(\pi - \theta, -\pi + \phi) = (-1)^l Y_l^m(\theta, \phi) \quad (2)$$

it follows that a spherical harmonic expansion of an intensity distribution may contain only even values of the angular momentum quantum number l . The fact that the intensity distribution is real, allows the restriction to a summation over just the so-called real spherical harmonics (RSHs) $S_l^m(\theta, \phi)$ defined by the combinations of spherical harmonics:

$$S_l^m(\theta, \phi) = \begin{cases} \frac{1}{\sqrt{2}} [Y_l^m(\theta, \phi) + (-1)^m Y_l^{-m}(\theta, \phi)] & m > 0 \\ Y_l^0(\theta, \phi) & m = 0 \\ \frac{1}{i\sqrt{2}} [Y_l^m(\theta, \phi) - (-1)^m Y_l^{-m}(\theta, \phi)] & m < 0 \end{cases} \quad (3)$$

where the set of RSH's with $m \geq 0$ form a set, whose ϕ dependence is of the form $\cos(m\phi)$, and the set with $m \leq 0$ likewise a set with ϕ dependence of the form $\sin(m\phi)$. If the reconstructed intensity distribution has a mirror plane, this may be chosen to be the $x-z$ plane, or the plane for which $\phi = 0$. Then (1) may be replaced by a summation over only the subset of RSHs for which $m \geq 0$, and we may take

$$I(q, \theta, \phi) = \sum_{l,m \geq 0} R_{lm}(q) S_l^m(\theta, \phi). \quad (4)$$

Since both the right hand side (RHS) and the left hand side (LHS) of the above equation are real, the coefficients $R_{lm}(q)$ may also be taken as real.

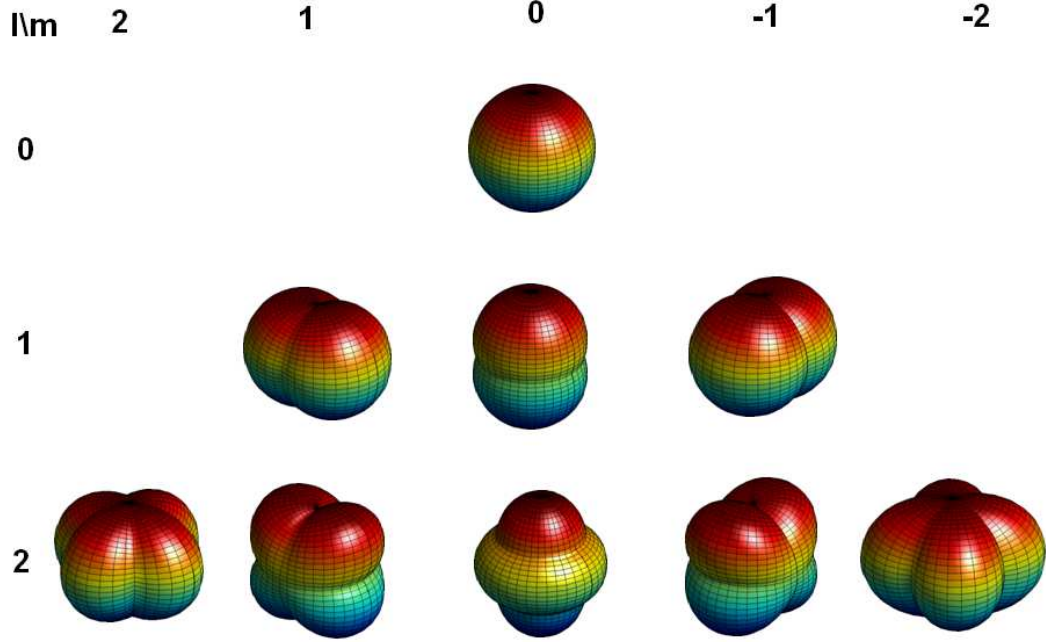


Fig. 1. Visualization of real spherical harmonics (RSHs) of angular momentum quantum numbers $l = 0, 1, \text{ and } 2$. The plots are made with MATLAB by an adaptation of software by Denise L. Chan (available from the Mathworks web site).

The 3D polar plots of Fig. 1 display the familiar forms of the RSHs for the values of $l = 0, 1, 2$. Further point group symmetries of $I(q, \theta, \phi)$ result in still further restrictions on allowed terms of the general expansion (1) above. When the 3D intensity distribution has icosahedral symmetry, for example, (1) may be replaced by

$$I(q, \theta, \phi) = \sum_l g_l(q) J_l(\theta, \phi), \quad (5)$$

where the quantities $J_l(\theta, \phi)$ are known as icosahedral harmonics (IHs), specified up to and including $l=30$ by only the angular momentum quantum number l . Since the orientation of our reconstructed 3D intensity distribution in the frame of reference of the particle may be chosen arbitrarily, the $x-z$ plane may be chosen to be the mirror plane, allowing the IHs (5) to be constructed from just the RSHs of positive m , i.e.

$$J_l(\theta, \phi) = \sum_{m \geq 0} a_{lm} S_l^m(\theta, \phi) \quad (6)$$

where the coefficients a_{lm} are the real numbers for normalized RSHs tabulated by e.g. Jack and Harrison (1975) [10], the ones for the lowest allowed even values of l being reproduced in Table 1. Since the IHs involve a sum over the magnetic quantum number, at least up to $l = 30$, they depend on the quantum number l only. The forms of the icosahedral harmonics of lowest even degree, $l=0,6,10,12$, and 16 are illustrated in Fig. 2 using the same 3D polar plots.

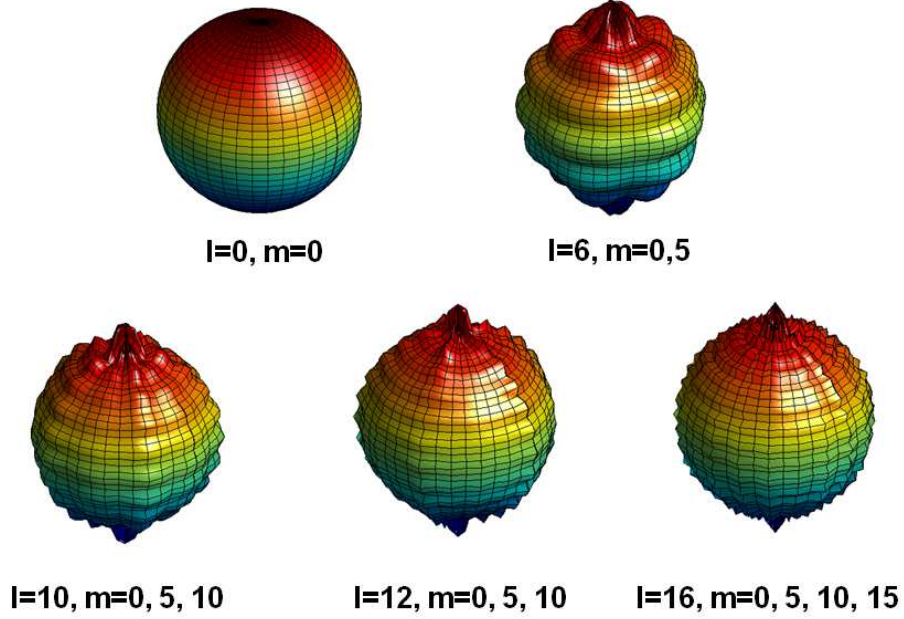


Fig. 2. Icosahedral harmonics of angular momentum quantum number $l = 0,6,10,12$ and 16. Each is a linear combination of the RSH's of the magnetic quantum numbers indicated. Visualization by the same software as Fig. 1

Note that since the RSH's $S_l^m(\theta, \phi)$ are orthonormal with respect to integrations over spherical shell, the icosahedral harmonics $J_l(\theta, \phi)$ will also be orthonormal with respect to the same integration provided

$$\sum_m a_{lm}^2 = 1, \quad \forall l. \quad (7)$$

This condition is clearly satisfied by the coefficients in Table 1.

3. Reconstructing the Diffraction Volume

The average angular correlations amongst the resolution rings of the different measured diffraction patterns contain information about the 3D diffraction volume of a single particle. Such angular correlations are defined by

$$\begin{aligned} C_2(q, q', \Delta\phi) &= \frac{1}{N_p} \sum_p \sum_{n=0}^{N-1} I_p(q, \phi_n) I_p(q', \phi_n + \Delta\phi) \\ &= \frac{1}{N_p} \sum_p \frac{1}{N} \sum_{m=0}^{N-1} I_m(q) I_m(q')^* \exp(-im\phi_n) \end{aligned} \quad (8)$$

where I_p is the intensity on diffraction pattern p , N_p is the number of available diffraction patterns from random orientations of the particle, ϕ_n is the n -th of N discrete values of ϕ , and

$$I_m(q) = \sum_{n=0}^{N-1} I_p(q, \phi_n) \exp(im\phi_n) \quad (9)$$

the angular Fourier transform of each resolution ring of the p -th diffraction pattern. Indeed the fastest way to calculate the average angular correlation $C_2(q, q', \Delta\phi)$ is to exploit the cross-correlation theorem by performing the angular Fourier transform (9) of each individual diffraction pattern, take the product of the Fourier transform and its complex conjugate followed by the inverse transform, and to average the results over the diffraction patterns ((9) plus the second equality of (8)).

It has been shown [6] that if the data from enough diffraction patterns of randomly oriented identical particles are averaged,

$$C_2(q, q', \Delta\phi) = \sum_l F_l(q, q', \Delta\phi) B_l(q, q') \quad (10)$$

where

$$F_l(q, q', \Delta\phi) = \frac{1}{4\pi} P_l[\cos\theta(q) \cos\theta(q') + \sin\theta(q) \sin\theta(q') \cos(\Delta\phi)] \quad (11)$$

where P_l is a Legendre polynomial of order l ,

$$\theta(q) = \pi/2 - \sin^{-1}(q/2\kappa), \quad (12)$$

κ is the wavenumber of the incident beam, and

$$B_l(q, q') = \sum_m I_m^*(q) I_m(q') \quad (13)$$

Since in Eq.(10), the LHS may be found from experiment, and $F_l(q, q', \Delta\phi)$ is a known mathematical function, $B_l(q, q')$ may be found by solving this equation. Due to its form, $B_l(q, q')$ contains information about the 3D diffraction volume of the particle via the spherical harmonic expansion coefficients $I_m(q)$. Because the RSHs are related to the regular spherical harmonics by a unitary transformation, one may also write

$$B_l(q, q') = \sum_m R_{lm}(q) R_{lm}(q'). \quad (14)$$

This is a more convenient form since all quantities in this equation are real. If the $R_{lm}(q)$ coefficients may be found from deduced values of $B_l(q, q')$, the expression (4) is just as convenient for reconstructing the 3D diffraction volume as (1).

However, finding the correct $R_{lm}(q)$'s from known $B_l(q, q')$'s is still a formidable task since it involves taking a matrix square root [6]. Such a square root is necessarily ambiguous by an orthogonal matrix which cannot be found from the $B_l(q, q')$'s alone. In principle, such an orthogonal matrix may be found from the so-called angular triple correlations [11] or by an iterative phasing algorithm that alternately satisfies constraints to the measured angular correlations and in the 3D space of the reconstructed intensity distribution [12].

When the particle under study is known to have a high degree of symmetry, like an icosahedral virus, this problem is greatly simplified. Comparing (4) and (5) with definition (6), one can deduce that, for a diffraction volume with icosahedral symmetry,

$$R_{lm}(q) = g_l(q) a_{lm} \quad (15)$$

Substituting (15) into (14) we see that one may write

$$B_l(q, q') = g_l(q)g_l(q') \sum_m a_{lm}^2 \quad (16)$$

and using (7) this may be simplified further to

$$B_l(q, q') = g_l(q)g_l(q') \quad (17)$$

We see here the great advantage of using IH's rather than RSHs for this problem of icosahedral symmetry. The sum over m in the RHS of (14) has disappeared completely in the RHS of (17)! The RHS of this equation is just the product of two scalars. A diffraction volume of icosahedral symmetry may be reconstructed via (5) if the coefficients $g_l(q)$ are known. Since the other quantities in (15) are real, it is clear that $g_l(q)$ may be chosen to be real. The magnitudes of the $g_l(q)$ coefficients may be found from the diagonal quantities $B_l(q, q)$ deduced from the intensity autocorrelations on resolution ring q via

$$|g_l(q)| = \sqrt{B_l(q, q)} \quad (18)$$

Thus, the only remaining task in determining the coefficients $g_l(q)$ is determining the signs of these real numbers. A simple way is to notice that the expression (5) for the intensity of a resolution shell of radius q in the 3D diffraction volume may be rewritten

$$I(q, \theta, \phi) = \sum_l |g_l(q)| \text{sign}[g_l(q)] J_l(\theta, \phi) \quad (19)$$

where the only unknown quantities in the RHS are the signs of $g_l(q)$. Since the only permitted values of the quantum number l of the icosahedral harmonic coefficients $g_l(q)$ of a diffraction volume are the even permitted values up to $l=30$, namely $l=0, 6, 10, 12, 16, 18, 20, 22, 24, 26, 28, \text{ and } 30$, we attempted to determine these signs by an exhaustive search over the $2^{12} \simeq 4000$ combinations of signs by finding the combination that minimized

$$\sum_{\theta, \phi} |I_-(q, \theta, \phi)| \quad (20)$$

where I_- are the negative values of I , for a chosen resolution shell q . The physical basis of this is simply that $I(q, \theta, \phi)$ has to be a positive definite quantity, and our best approximation to this is a function with a minimum sum of the magnitudes of negative values. As subsequent results show, this easily implemented prescription seemed accurate enough to find a good enough approximation to the correct signs of these coefficients for the chosen reference resolution ring. To maximize the number of non-negligible magnitudes $|g_l(q)|$ we chose a high-resolution resolution ring. In order to avoid almost all values $|g_l(q)|$ being very small, and thus subject to significant rounding-off errors, we found the best compromise to choose the reference ring to be one for which $q \simeq \frac{2}{3}q_{max}$, where q_{max} is the value of q for the outermost resolution shell.

From Eq. (17), we see that the icosahedral harmonic expansion coefficients of the same quantum number l , corresponding to a different resolution shell q' are related to the now known ones of resolution shell q by the simple quotient

$$g_l(q') = B_l(q, q')/g_l(q), \quad (21)$$

Thus, having found the coefficients $g_l(q)$ for a particular shell q , those of the other shells q' were determined from this simple quotient, involving the quantities $B_l(q, q')$ directly calculable from the average intensity cross correlations between different resolution rings on the measured

diffraction patterns. Thus the exhaustive search through all 2^{12} combination of signs needs to be performed only for a single resolution ring q .

A knowledge of the expansion coefficients for all the resolution shells should enable a reconstruction of the 3D diffraction volume via (5). If this intensity distribution is interpolated onto an oversampled [13] 3D Cartesian reciprocal-space grid, (q_x, q_y, q_z) , say, an iterative phasing algorithm [14] may be applied to reconstruct the 3D electron density of the scattering particle.

4. Numerical Tests

A central thesis of this paper is that the scattered intensity from an icosahedral particle may be represented by a sum of icosahedral harmonics. We first sought to verify this proposition by calculating first the spherical harmonic expansion coefficients of a simple icosahedral particle via the expression

$$A_{lm}(q) = i^l \sum_j f_j(q) j_l(qr_j) Y_{lm}(\hat{r}_j), \quad (22)$$

where $f_j(q)$ is the form factor of the j th atom, \mathbf{r}_j is its coordinate, and j_l is a spherical Bessel function of order l .

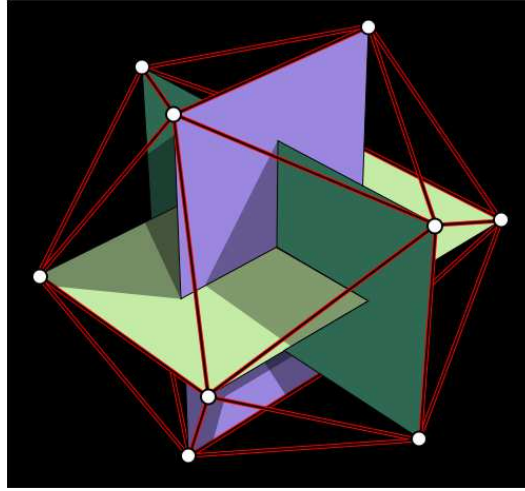


Fig. 3. Regular icosahedron [15]

For our initial tests we simulated the scattering from an artificial molecule of identical atoms at the vertices of a regular icosahedron (Fig. 3) of edge length 2 [15] (which we take to be to be in Å units, with Cartesian coordinates (also assumed to be in Å):

$$\begin{aligned} &(0, \pm 1, \pm \Phi) \\ &(\pm 1, \pm \Phi, 0) \\ &(\pm \Phi, 0, \pm 1) \end{aligned}$$

where Φ is the golden ratio $(1+\sqrt{5})/2$.

The resulting calculated values of the amplitudes A_{lm} (arbitrarily taking $f_j(q) = 1, \forall j$) for all possible values of l and m are listed in Fig. 4. Note that the amplitudes A_{lm} are all real, and that, for the values listed, they are non-zero only for $l=0$ and 6. The values for $l=1,2,3,4,5$, and 7 are all seen to be zero, corresponding to non-existing icosahedral harmonics for these values of l . Here too, all coefficients are zero except those for which $l=0$ or 6, and all non-zero

0 0	3.385138	0.000000	5 -3	-0.000000	0.000000
1 -1	-0.000000	0.000000	5 -2	-0.000000	0.000000
1 0	0.000000	0.000000	5 -1	0.000000	0.000000
1 1	-0.000000	0.000000	5 0	0.000000	-0.000000
2 -2	-0.000000	-0.000000	5 1	0.000000	0.000000
2 -1	0.000000	0.000000	5 2	-0.000000	0.000000
2 0	-0.000000	0.000000	5 3	-0.000000	0.000000
2 1	0.000000	0.000000	5 4	0.000000	-0.000000
2 2	-0.000000	-0.000000	5 5	-0.000000	-0.000000
3 -3	0.000000	-0.000000	6 -6	-2.592501	-0.000000
3 -2	0.000000	0.000000	6 -5	0.000000	0.000000
3 -1	-0.000000	0.000000	6 -4	-3.139675	-0.000000
3 0	0.000000	0.000000	6 -3	0.000000	-0.000000
3 1	-0.000000	0.000000	6 -2	3.845301	0.000000
3 2	0.000000	0.000000	6 -1	0.000000	0.000000
3 3	0.000000	-0.000000	6 0	1.678227	0.000000
4 -4	-0.000000	0.000000	6 1	0.000000	0.000000
4 -3	0.000000	0.000000	6 2	3.845301	0.000000
4 -2	0.000000	0.000000	6 3	0.000000	-0.000000
4 -1	0.000000	0.000000	6 4	-3.139675	-0.000000
4 0	0.000000	0.000000	6 5	0.000000	0.000000
4 1	0.000000	0.000000	6 6	-2.592501	-0.000000
4 2	0.000000	0.000000	7 -7	0.000000	-0.000000
4 3	0.000000	0.000000	7 -6	-0.000000	0.000000
4 4	-0.000000	0.000000	7 -5	0.000000	0.000000
5 -5	-0.000000	-0.000000	7 -4	0.000000	0.000000
5 -4	0.000000	-0.000000	7 -3	0.000000	0.000000

Fig. 4. Calculated values of the A_{lm} coefficients (arbitrarily taking $f_j(q) = 1, \forall j$) assuming 12 identical atoms at the vertices of a regular icosahedron. The first two entries in each column in each line are the l and m values. The next two are the real and imaginary parts of $A_{lm}(q)$. It will be seen that all coefficients are zero except those for which $l=0$ or 6, and that all non-zero coefficients are real.

coefficients are real. Note that this result will be true for any icosahedral orientation since the a rotation matrix (Wigner D-matrix) will mix only amplitudes of different magnetic quantum number corresponding to the same angular momentum l . The z-axis of the simple icosahedron used for this test is a 2-fold rotation axis, not 5-fold, unlike e.g. Fig. 2 above, or Table 1 below. This is why the amplitudes corresponding to every other value of m are non zero for $l=6$ rather than every integer multiple of 5, when z is chosen to be a 5-fold axis.

Of greater interest for our method are the allowed values of L for the coefficients, I_{LM} , of the spherical harmonic expansions of the scattered intensity. Since

$$I(\vec{q}) = |A(\vec{q})|^2, \quad (23)$$

it must follow that if $A(\mathbf{q})$ has icosahedral symmetry, so must $I(\mathbf{q})$. However, this is not entirely obvious from the relationship between the two sets of coefficients

$$\begin{aligned} I_{LM}(q) &= \sum_{lm;l'm'} A_{lm}(q)A_{l'm'}^*(q) \int Y_{lm}(\hat{\mathbf{q}})Y_{l'm'}^*(\hat{\mathbf{q}})Y_{LM}^*(\hat{\mathbf{q}})d\hat{\mathbf{q}} \\ &= \sum_{lm;l'm'} A_{lm}(q)A_{l'm'}^*(q) \int Y_{lm}^*(\hat{\mathbf{q}})Y_{l'm'}(\hat{\mathbf{q}})Y_{LM}(\hat{\mathbf{q}})d\hat{\mathbf{q}} \\ &= \sum_{lm;l'm'} A_{lm}(q)A_{l'm'}^*(q) \sqrt{\frac{(2l'+1)(2L+1)}{4\pi(2l+1)}} C_{l'0l0}^{l0} C_{l'm'LM}^{lm} \end{aligned} \quad (24)$$

where $C_{l'm'LM}^{lm}$ is a Clebsch-Gordan coefficient [16]. According to the usual theory of the vector addition of angular momenta, the allowed values of L are all integers in the range from $|l-l'|$ to $l+l'$, with no obvious indication that $L=1,2,3,4,5$, and 7, for instance, are forbidden. However, a straightforward evaluation of the $I_{LM}(q)$ coefficients via (24) reveals this to be the case, as is seen by the tabulated values of these coefficients in Fig. 5.

0 0	29.638449	0.000000			
1 -1	-0.000000	0.000000			
1 0	0.000000	0.000000			
1 1	-0.000000	0.000000			
2 -2	-0.000000	-0.000000			
2 -1	0.000000	0.000000			
2 0	-0.000000	0.000000			
2 1	0.000000	0.000000			
2 2	-0.000000	-0.000000			
3 -3	0.000000	-0.000000			
3 -2	0.000000	0.000000			
3 -1	-0.000000	0.000000			
3 0	0.000000	0.000000			
3 1	-0.000000	0.000000			
3 2	0.000000	0.000000			
3 3	0.000000	-0.000000			
4 -4	-0.000000	0.000000			
4 -3	0.000000	0.000000			
4 -2	0.000000	0.000000			
4 -1	0.000000	0.000000			
4 0	0.000000	0.000000			
4 1	0.000000	0.000000			
4 2	0.000000	0.000000			
4 3	0.000000	0.000000			
4 4	-0.000000	0.000000			
5 -5	-0.000000	-0.000000			
5 -4	0.000000	-0.000000			
5 -3	-0.000000	0.000000			
5 -2	-0.000000	0.000000			
5 -1	0.000000	0.000000			
5 0	0.000000	-0.000000			
5 1	0.000000	0.000000			
5 2	-0.000000	0.000000			
5 3	-0.000000	0.000000			
5 4	0.000000	-0.000000			
5 5	-0.000000	-0.000000			
6 -6	-30.398445	-0.000000			
6 -5	0.000000	0.000000			
6 -4	-36.814346	-0.000000			
6 -3	0.000000	-0.000000			
6 -2	45.088181	0.000000			
6 -1	0.000000	0.000000			
6 0	19.678095	0.000000			
6 1	0.000000	0.000000			
6 2	45.088181	0.000000			
6 3	0.000000	-0.000000			
6 4	-36.814346	-0.000000			
6 5	0.000000	0.000000			
6 6	-30.398445	-0.000000			
7 -7	0.000000	-0.000000			
7 -6	-0.000000	0.000000			
7 -5	0.000000	0.000000			
7 -4	0.000000	0.000000			
7 -3	0.000000	0.000000			

Fig. 5. Same as Fig. 4, except for values of the $I_{LM}(q)$ coefficients calculated by Eq. (24) from the $A_{lm}(q)$ values in Fig. 4.

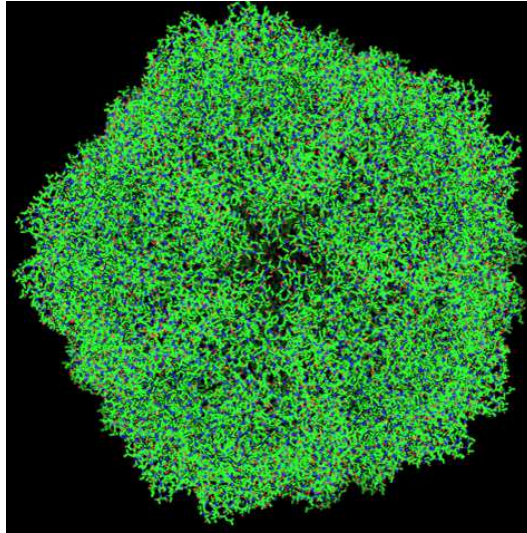


Fig. 6. Top part of the structure of the satellite tobacco necrosis virus (STNV) viewed down its 5-fold axis (from structure data in PDB entry: 2BUK)

We next tested this on a realistic model of the small icosahedral virus, satellite tobacco necrosis virus (STNV) whose atomic coordinates are deposited in the protein data bank under entry 2BUK (Fig. 6). We calculated $A(\mathbf{q})$ from the usual structure factor expression

$$A(\vec{q}) = \sum_j f_j(q) \exp(i\vec{q} \cdot \vec{r}_j) \quad (25)$$

and constructed the diffraction volume from (23). By integrating over spherical shells of $I(\vec{q})$ we evaluated the spherical harmonic expansion coefficients of the 3D diffraction volume of STNV from

$$I_{lm}(q) = \int I(\vec{q}) Y_{lm}(\hat{\mathbf{q}}) d\hat{\mathbf{q}}, \quad (26)$$

where $\hat{\mathbf{q}}$ is the unit vector \vec{q}/q , with this integration conveniently performed by Gaussian quadrature [17]. Plots of the real and imaginary parts of I_{lm} in Fig. 7 clearly show the same trend of vanishing components corresponding to $l = 1, 2, 3, 4, 5$, and 7 and in addition vanishing components for $l = 8, 9, 11, 13, 14$, and 15, exactly consistent with the tabulated values of icosahedral expansion coefficients in Table 1. What is more, it was found that

$$(-1)^m I_{l(-m)}(q) = I_{lm}(q), \quad (27)$$

the precise condition for the reality of the $R_{lm}(q)$ coefficients of the RSHs, and hence of the icosahedral harmonic expansion coefficients $g_l(q)$ via (15).

Since this result is a consequence of the icosahedral symmetry of the diffraction volume $I(\mathbf{q})$, it is to be expected of the diffraction volume of all icosahedral viruses (assuming the protein coat to be the dominant scatterer). In view of (13) this must mean that the $B_l(q, q')$ coefficients computed from the data of diffraction patterns of random orientations of all icosahedral particles must all have vanishing values for $l = 1, 2, 3, 4, 5, 7, 8, 9, 11, 13, 14, 15, \dots$, thus providing a very simple test of whether the diffraction patterns measured in a ‘‘diffract and destroy’’ experiment with a FEL are from an icosahedral particle.

Assuming this is indeed found to be approximately true in practice (even the so-called icosahedral viruses may have appendages which break the icosahedral symmetry of the protein coat, and of course the genetic material inside the protein coat would not be expected to have this symmetry. However, if the bulk of the material of the virus may be assumed to constitute the protein coat, this must be approximately the case). The icosahedral structure of the protein coat may be found by an analysis of the large $l = 0, 6, 10, 12, 16, \dots$ $B_l(q, q')$ coefficients extractable from the average angular correlations of the diffraction data.

5. Reconstruction of STNV from Simulated Diffraction Patterns

We next attempted a reconstruction of satellite tobacco necrosis virus (STNV) from diffraction patterns simulated for directions of incidence on a single particle from a uniform angular distribution in $SO(3)$ [18]. For the model of STNV we took the data of the biological assembly of STNV from PDB entry 2BUK. Due to the large number of atoms in this biological assembly ($\sim 100,000$), the most convenient way to do this was to take slices through a precalculated 3D diffraction volume of this structure. Average angular correlations of these simulated diffraction patterns were calculated by the formulae (8) and (9). and the $B_l(q, q')$ coefficients were calculated from these by inverting Eq. (10).

For the 10,000 simulated diffraction patterns in our test, this process took about a quarter of an hour on a single processor on a desktop computer. In a real experiment, one may have to deal with perhaps 100 times as many diffraction patterns, with more pixels per pattern, so the processing time could be several orders of magnitude greater. However, the bulk of the time will be spent in generating the average angular correlations $C_2(q, q', \Delta\phi)$ (8), a process

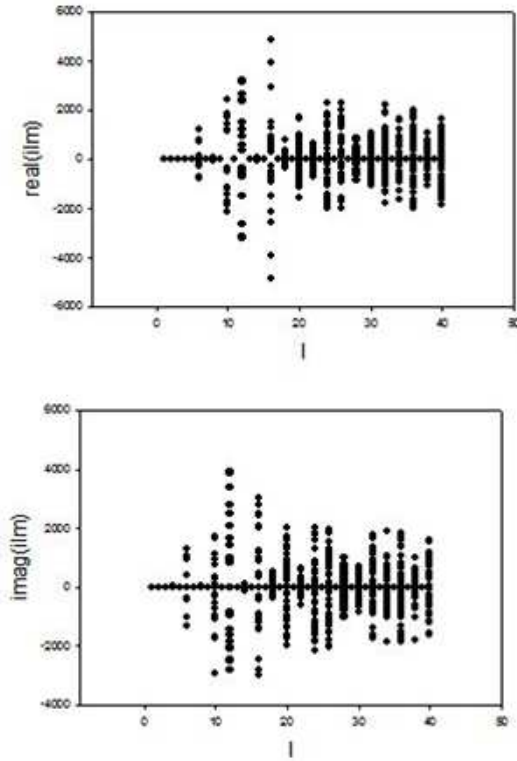


Fig. 7. Real and imaginary parts of the $I_{lm}(q)$ coefficients calculated from the computed diffraction volume of STNV. Each dot represents a value of the (lm) pair. Note that these coefficients are largely absent for $l=1,2,3,4,5,7,8,9,11,13,14,15$.

which easily lends itself to parallelization, since subsets of the diffraction patterns may be averaged by separate computer processors, and the averages themselves subsequently averaged. Nevertheless, this process of reduction of terabytes (TB) of measured experimental data is probably the most computer-resource intensive part of our method. Having thus reduced our data to a set of $B_l(q, q')$ coefficients for a set of 30 values of l , and 61 values of q (and q'), we were left with a set of $30 \times 61 \times 61$ real numbers which formed the input to our reconstruction algorithm. This required about a MB of storage/memory. In a real experiment also, our method requires the million-fold reduction of the TB of data to a MB of floating-point (real) numbers that form the input to our reconstruction algorithm. It is recommended that this data reduction be performed at the site of the data to reduce by a million-fold or so the quantity of data that needs to be transmitted over the internet to the site where the image reconstruction is performed. At current rates, the transmission of Terabytes of data over the internet could take several weeks, whereas the time for the transmission of a MB of data could be measured in seconds. In addition this process of data reduction is expected to result in considerable noise-reduction of the raw data though averaging [19].

Since the $B_l(q, q')$ coefficients are related to the expansion coefficients $R_{lm}(q)$ of the real spherical harmonics (which satisfy the same selection rule on l as do the expansion coefficients $I_{lm}(q)$ of the regular spherical harmonics), it would be expected that the $l = 0, 6, 10, 12, 16, 18, 20, 22, 24, 26, 28, 30$ elements of these coefficients are dominant. This was found to be the case for our simulations of STNV. Some of the larger, predominantly icos-

hedral, viruses may have appendages like the unique vertex and “hair” of the mimivirus [20], or the spike from a unique vertex of the chlorella virus [21]. Indeed, with values of these coefficients extracted from experimental single-particle diffraction patterns from an unknown particle, the satisfaction of this selection rule would be an excellent test of the degree to which the particle is icosahedral. Inclusion of only the large $l = 0, 6, 10, 12, 16, \dots$ of the $B_l(q, q')$ coefficients in the reconstruction algorithm consistent with icosahedral symmetry is equivalent to finding the closest icosahedral approximation to the structure.

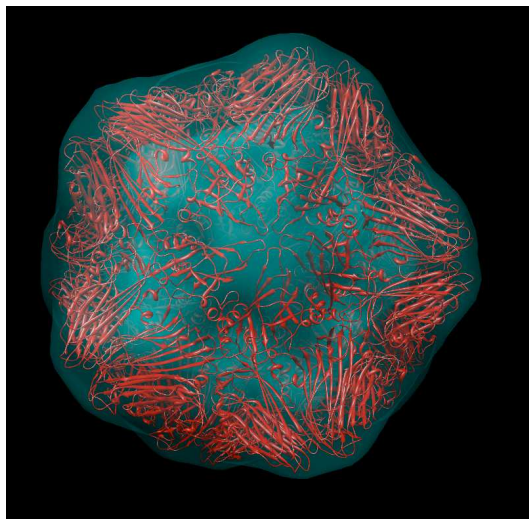


Fig. 8. Reconstructed image from the diffraction volume of a single STNV particle computed directly from a structure factor calculation. STNV is about 20 nm in diameter. The figure depicts a view of the icosahedron close down its 5-fold rotation axis. The reconstruction assumed a maximum value of q , q_{max} , of about 4.7 nm^{-1} , implying a resolution of $\sim 1.3 \text{ nm}$. Both the outer and inner surfaces of the virus capsid are apparent in this representation. A ribbon diagram of the structure in PDB entry 2BUK is seen to fit within this capsid.

The procedure described in section 3 was then followed to reconstruct a 3D diffraction volume, consisting of set of scattered intensities $I(q_x, q_y, q_z)$ over 3D reciprocal space as a function of the reciprocal-space coordinate $\vec{q} \equiv (q_x, q_y, q_z)$. In our simulations, we took this to be a $61 \times 61 \times 61$ array of real numbers. The computer time for this process was almost ridiculously short, amounting to no more than a few seconds on a single-processor desktop computer.

The final step is the recovery of a 3D electron density of the particle. This may be done by a standard iterative phasing algorithm. We used the “charge flipping” algorithm of Oszlányi and Sütő [22, 23]. In order to judge the accuracy of our algorithm in recovering the 3D diffraction volume, we performed this recovery of the 3D electron density from both the diffraction volume $I(\mathbf{q})$ calculated directly from the STNV structure factors (Fig. 8), and also by our algorithm from the $B_l(q, q')$ coefficients (Fig. 9), which may be computed from the measured data of the FEL diffraction patterns from random particle orientations. The similarity of the reconstructed images of Figs. 8 and 9 was a further indication of the validity of the method of image reconstruction from the quantities $B_l(q, q')$ derivable from the average angular correlations. The fact that the reconstructed image consists of a thin protein shell is also seen from the slice perpendicular to a 5-fold rotation axis through the reconstructed image of Fig. 9 depicted in Fig. 10. In the case of all three figures, a ribbon representation of the structure from

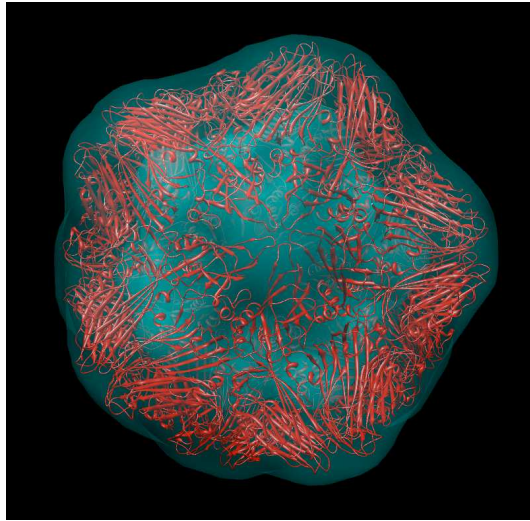


Fig. 9. Same as Fig. 8 except that the diffraction volume was reconstructed from the average of angular correlations on 10,000 diffraction patterns of STNV from uniformly distributed directions over $SO(3)$. The reconstructed electron density is seen to be remarkably similar to that in Fig. 8.

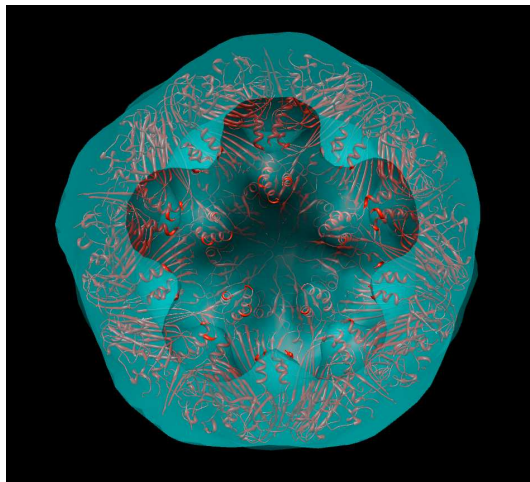


Fig. 10. Same as Fig. 9 except that image displayed is a cut perpendicular to the 5-fold axis of the virus. The 5-fold symmetry of both the external and internal surfaces of the capsid in this projection are clearly visible.

the biological assembly of the STNV virus from the same PDB structure used to simulate the diffraction patterns is superimposed on the semi-transparent electron density to show the excellence of the reconstruction. It should be emphasized that nowhere in our theory is it assumed that the structure consists of a thin protein shell, unlike the so-called shell model that has been used in the SAXS analysis of virus capsids [24]. In our case, the existence of a shell is deduced by an iterative phasing algorithm from the analysis of data from diffraction patterns of random particle orientations without any assumptions on our part.

6. Beyond the Icosahedral Approximation

Satellite tobacco necrosis virus (STNV) is an example of a virus with a perfectly icosahedral protein coat [25]. A host cell gets access to the genetic material of this virus by ingesting it whole and dissolving its protein coat.

Many of the larger viruses are only approximately icosahedral: they often have appendages, such as a neck sticking out of the coat that is used to inject the genetic material inside the coat into a host cell whose protein making capability is hijacked by the virus DNA or RNA.

An ultimate reconstruction algorithm should be able to reconstruct these non-icosahedral parts of the structure in addition to the icosahedral part. The above procedure has determined the icosahedral harmonic expansion coefficients $g_l(q)$ that best fit the measured quantities $B_l(q, q')$. Any deviations from these values are due to the non-icosahedral parts of the structure. Any differences between the experimental values of $B_l(q, q')$ and $g_l(q)g_l(q')$ may be written

$$\delta B_l(q, q') = \sum_m a_{lm} \{g_l(q)\delta R_{lm}(q') + \delta R_{lm}(q)g_l(q')\} + \delta R_{lm}(q)\delta R_{lm}(q'), \quad (28)$$

in terms of $\delta R_{lm}(q)$, the extra contribution to the RSH expansion coefficients due to deviations from icosahedral symmetry. Note that for (l, m) combinations not associated with icosahedral harmonics, e.g. those for which there is no entry in a list like Table 1, the terms a_{lm} will be zero, and only the quadratic terms in δR_{lm} will survive in (28). Determination of the $\delta R_{lm}(q)$ coefficients which optimize the agreement the theoretical expression (28) and the measured values will enable the construction of a better estimate of a single-particle diffraction volume via

$$I(\vec{q}) = \sum_{lm} \{g_l(q)a_{lm} + \delta R_{lm}(q)\} S_{lm}(\hat{\mathbf{q}}). \quad (29)$$

The presence of the correction terms $\delta R_{lm}(q)$, which have no symmetry restrictions (apart from Friedel symmetry) will allow the diffraction volume calculated by this formula to include deviations from icosahedral symmetry.

Application of an iterative phasing algorithm to an oversampled diffraction volume calculated by this expression will enable the determination of the full structure of the virus, including any appendages that break the approximate icosahedral symmetry.

7. Discussion

The remarkable similarity of the reconstructed electron densities of Figs. 8 and 9, and the fit of the latter to the model of STNV from the PDB file, are indications of the correctness of the method of reconstruction of the 3D diffraction volume from the average angular correlations of the 10,000 simulated diffraction patterns of STNV. We calculated from these the $B_l(q, q')$ coefficients for all values of l from 0 to 30. We found good agreement with the selection rule on the l coefficients in which the sizes of the $B_{q, q'}$ coefficients for all odd values of l were small (due to Friedel, or inversion, symmetry) and in addition the even values $l=2, 4, 8,$ and 14 were also small, due to the icosahedral symmetry of the 3D diffraction volume of a single particle. We included $g_l(q)$ coefficients for the non-negligible $B_l(q, q')$ coefficients up to $l=30$

(up to which value the icosahedral harmonic expansion coefficients depend on the l quantum number only). If q_{max} is the maximum value of the reciprocal-space coordinate q up to which the reconstruction is valid, conventional wisdom [26] suggests that l_{max} and q_{max} should be related by

$$q_{max}R = l_{max}, \quad (30)$$

where R is the radius of the particle. Taking

$$q_{max} = 2\pi/d \quad (31)$$

where d is the resolution. Substituting (31) into (30) and rearranging, we find that

$$d/R = 2\pi/l_{max} \simeq 1/5. \quad (32)$$

STNV has a radius of ~ 100 Å suggesting a resolution of about 20 Å. In practice we found that increasing q_{max} a further 50% or so, while keeping l_{max} fixed at 30 seemed to improve the quality of the reconstructed image. Presumably because up to about $1.5q_{max}$ the spherical harmonic expansion coefficients of l greater than 30 remain small.

It should be emphasized this is not necessarily an absolute limit of the resolution obtainable with the use of icosahedral harmonics. The higher order harmonics, at least up to $l=44$, have been tabulated by Zheng *et al.* [24]. At least up to this value, the degeneracy of the icosahedral harmonics characterized by a particular value of l is no more than two. Although the algorithm for recovering the expansion coefficients of such degenerate harmonics from the experimental data is a little more complicated, it seems far from an insuperable problem.

The images in Figs. 8 to 9 were computed by an iterative phasing algorithm [22, 23] from a reciprocal-space distribution of intensities oversampled [13] by a factor of ~ 2 with respect to the size of STNV, up to a q_{max} value of ~ 0.47 Å⁻¹ (a $61 \times 61 \times 61$ array), implying a resolution of about 13 Å, and a d/R ratio closer to 1/8. Further, the images of Fig. 8-10 reveal this coat to be hollow. The slice (Fig. 10) through the reconstructed image perpendicular to the 5-fold axis reveals both external and internal surfaces of 5-fold rotational symmetry. The revelation of the hollow nature of the protein coat is of course an extra feature contained in the 3D intensity distribution above and beyond the assumed icosahedral symmetry. It is revealed by the iterative reconstruction algorithm used [22, 23] due to the particular variation of the $B_l(q, q')$ coefficients with the radial reciprocal-space coordinates q and q' .

Some the advantages of this method of analysis of single particle diffraction patterns from unknown particle orientations compared with other proposed algorithms [4, 5] should be pointed out. Since it has been shown [7, 27, 12, 19, 28], that the angular correlations of multiple identical particles in arbitrary orientations are essentially identical to those from a single particle, the method we have described is equally applicable to droplets containing multiple particles injected into the XFEL [29] as to the injection of single particles in random orientations. Thus there is no need to discard diffraction patterns from multiple particle hits.

Since the inputs to our algorithm are not the direct photon counts, but rather the average of the angular correlations between intensities of the *same* diffraction patterns, it is insensitive to shot-to-shot fluctuations between the diffraction patterns, as may be caused by intensity variations of the incident X-ray beam or, for example, by the number of particles scattering a particular X-ray pulse.

The raw experimental data is likely to consist of $\sim 10^6$ diffraction patterns, each of $\sim 10^6$ pixels. Thus the raw experimental data will require TB of storage. Of course, this is very noisy data, and the structural information content is much less than this. The averaging of the angular correlations that we perform may be regarded as a form of data averaging that results in information concentration and noise reduction. Even if the number of values of q chosen is, say,

61, and these coefficients are evaluated for, say, 30 values of l , the total number of these (real) coefficients will be only of the order of 100,000, requiring less than a MB of storage. This data reduction is best performed at the site of the data to allow the transfer of a million times less data over the internet to the site of image reconstruction. The reconstruction of 3D images of the quality of Figs. 8-10 from a properly constructed set of $B_l(q, q')$ coefficients is extraordinarily rapid. In our calculations, reconstruction of an array of $I(q_x, q_y, q_z)$ values representing a 3D diffraction volume at reciprocal-space coordinates $\vec{q} \equiv (q_x, q_y, q_z)$ on a $61 \times 61 \times 61$ Cartesian grid took just a few seconds on a single Intel Q6600 processor, using an Intel Fortran compiler. The reconstruction of real-space images of the quality of Figs. 8-10 from this array by means of a “charge flipping” algorithm [22, 23] took a further 4 minutes for 200 iterations on a laptop PC.

Of course, the averaging of the data from the different diffraction patterns assumes they all arise from copies of the particle in different orientations (as does the technique of small angle X-ray scattering, SAXS, for example). In order to distinguish between different conformations of the individual molecules, it may be necessary to operate on the entire ensemble of all the measured diffraction patterns. One of the disadvantages of such methods is the need to operate on single-particle diffraction patterns and thus, unlike with our method, diffraction patterns from multiple hits need to be removed. Such methods also face the problem of the uncertain normalization of incident intensities between successive pulses of incident radiation. Also, in contrast to our method, such techniques may require the transfer of perhaps TB of data over the internet to the site of the data performing the analysis, which needs to be equipped with a cluster of computers performing parallel computations.

8. Conclusions

When reconstructing the structure of a virus from “diffract and destroy” type single-particle diffraction experiments proposed for the free electron laser [1], one may exploit the dictum of Caspar and Klug [9] that “there are only a limited number of efficient designs possible for a biological container which can be constructed from a large number of identical protein molecules, The two basic designs are helical tubes and icosahedral shells”. We offer here a solution for the case of icosahedral viruses. For those viruses which are substantially, though not completely icosahedral, the method proposed is expected to be useful nonetheless for initially reconstructing the approximate icosahedral structure. The deviations from this structure can then be found by a perturbation theory which does not impose this symmetry.

The input to the algorithm is data from diffraction patterns of randomly oriented identical particles (where the particle orientations are unknown) in the form of the average of the angular correlations. As a consequence of any approximate icosahedral symmetry of the scattering particles, the angular momentum decomposition of the angular correlations contains only a few dominant contributions from low values of the angular momenta.

This immediately suggests a simple test of whether the experimentally measured data are from the scattering by an icosahedral object. If so, the components of the quantities $B_l(q, q')$, derivable from the angular correlations, should have much smaller values for $l=1,2,3,4$, and 5 than for $l=0$ and $l=6$, for example. What is more, as we have shown in this paper, the coefficients $g_l(q)$ of the icosahedral harmonic expansion of the 3D diffraction volume of the particle may be derived from the $B_l(q, q')$ data and a positivity condition on the intensities of the 3D diffraction volume. This will be the case even if the individual diffraction patterns are a result of scattering from more than one particle, so there will be no need to discard the diffraction patterns from multiple particles.

Having obtained the coefficients of an icosahedral harmonic expansion, the 3D diffraction volume may be reconstructed as a sum over these icosahedral harmonics. By definition, the

resulting diffraction volume will have icosahedral symmetry. If this is constructed at a grid that is oversampled by a factor of 2 in each dimension, we have shown that a “charge flipping” algorithm with no fixed support constraint is able to reconstruct a 3D image of the particle. We find that this procedure not only reconstructs an icosahedral shape for the particle, in simulations for the satellite tobacco necrosis virus (STNV) it even reveals the hollow nature of the protein coat.

We acknowledge helpful discussions with Profs. Abbas Ourmazd and John Spence, and financial support from DOE grant No. de-sc0002141.

Table 1. Expansion coefficients of the lowest even degree icosahedral harmonics with z-axis chosen to be the 5-fold rotation axis. For the list up to $l=30$, see e.g. [10]. Note the rows are characterized by l and the columns by m .

$l \backslash m$	0	5	10	15	20
0	1.0				
6	0.531085	0.847318			
10	0.265539	-0.846143	0.462094		
12	0.454749	0.469992	0.756513		
16	0.334300	-0.493693	-0.634406	0.491975	
18	0.399497	0.450611	0.360958	0.712083	
20	0.077539	-0.460748	0.747888	-0.231074	0.411056